Research Article

Synergic effect of montmorillonite and microcrystalline cellulose on the physicochemical properties of rice husk/PVC composite

Nipu Dutta[1] · **Tarun Kumar Maji**[1]

Received: 26 September 2019 / Accepted: 12 February 2020 / Published online: 18 February 2020

Abstract
Rice husk, an agricultural waste material, was tried to make value added by preparing composite with microcrystalline cellulose and montmorillonite by melt blending process in different proportions. The interaction among the components was studied by Fourier transform infrared spectroscopy and X-ray diffractometry. The mechanical and thermal properties were studied through universal testing machine, dynamic mechanical analyzer and thermogravimetr ic analyzer. Scanning electron microscopy and transmission electron microscopy were used to analyze the surface morphology of the composites. Among the various composition the better synergistic effect was observed in composite PRMCC2 with 2 phr MCC and 3 phr MMT. Along with thermal and mechanical properties, PRMCC2 also showed better flame retardancy and water-resistant properties.

Keywords Rice husk · PVC · Nanocomposites · Microcrystalline cellulose · Mechanical properties

1 Introduction

Cellulose-based plant filler or fibre is one of the most explored topics for the researchers of the present generation. Natural fibres have gained popularity over the conventional reinforcing materials due to the advantages provided by the natural filler [1, 2]. Conventional fibres used in fibre reinforced materials (FRP), are gradually replaced by natural fibres [3]. The natural fibre based polymer composite can be used in different applications due to the advantages such as low cost, high strength, low weight and easy processability [4–7]. Natural fibre based composites find wide application in automobile sectors [8–10].

Rice husk (RH) is one of the lignocellulosic biomasses which is widely produced by agriculture-based industries in India. It is generally treated as a waste and used as bedding material for cattle (animals), or landfilling material [11–13]. RH was also utilized as a source for extraction of different advance material like silicon, carbon etc. [14, 15] and as a material for metal–matrix composites [16, 17]. The waste RH can be explored as a reinforcing agent in polymer composite. Addition of RH in the composite will not only increase the properties of the composite but also decrease the cost of production of the polymer composite.

Cellulose-based reinforcement material shows good applicability along with excellent thermal and mechanical properties compared to other inorganic fillers [18]. Cellulose is comparatively easy to process due to its nonabrasive property, which initiates better filling levels resulting in significant cost saving [19]. With the development in research of cellulose, different forms of cellulose fibres are obtained such as microfibrils and nano whiskers [20]. These fibres have better mechanical properties compared to other commonly used reinforcing fillers. Microcrystalline cellulose (MCC), a famous reinforcing agent, closely resembles cellulose nanowhiskers [21]. MCC can be prepared easily from agricultural cellulose [22], and it has varied application in the field of cosmetics, medical and food processing industries [23]. Use of MCC as a reinforcing agent in polymer composite shows better tensile

✉ Tarun Kumar Maji, tkm@tezu.ernet.in | [1]Department of Chemical Sciences, Tezpur University, Napaam 784028, India.

strength and young modulus [24]. In order to overcome the limitations such as poor flow characteristics and less bulk density associated with MCC, different additives like starch, calcium carbonate, montmorillonite etc. are added to it [25–28].

Hybrid composite, which is prepared by combination of more than one reinforcing agent, showed enhancement properties compared to the individual reinforcing agent [29–31]. The hybridization of natural filler and nanofiller not only increases the mechanical properties but also reduces the water absorption properties of the composite [32]. Introduction of layered silicate nanomaterial to the polymer matrix enhances properties like modulus, toughness, strength and flammability compared to the virgin polymers [33]. MMT, a low cost and environment–friendly layered silicate nanofiller used in many application and industrial fields [34–36].

PE-g-MA can be used as a compatibilizer and plays an important role to improve the interaction among the components specially between PVC and RH. Here the compatibilizer act as a bridge between the hydrophobic part of PVC and hydrophilic part of RH, MCC and MMT. The polyethylene chain of compatibilizer will interact with the hydrocarbon part of PVC and the anhydride portion will interact with the hydroxyl groups of RH, MCC and MMT.

Polyvinyl chloride (PVC), which is second most-produced thermoplastic after polyolefin is used widely in different applications. The performance of the PVC can be improved by modifying the structure and properties through the introduction of various additives [37]. The fragmentation of PVC based composite can be enhanced by increasing the percentage of natural, low-cost filler within the matrix. Keeping these in mind, nanocomposites have been prepared by melt blending of PVC, RH, MCC and MMT. The percentage of MCC and MMT has been varied keeping other components (PVC, RH, PE-g-MA, Lead carbonate) constant. The combined effect of MCC and MMT on the physicochemical properties such as mechanical, thermal, water absorption, flame resistance has been studied and reported.

2 Experimental

2.1 Materials and methods

PVC (Grade: SPVC FS: 6701) was supplied by Finolex Industries Ltd. (Pune, India). Basic Lead Carbonate (LC) and Dibutyl phthalate (DBP) were obtained from G.S. Chemical Testing Lab & allied industries (Mumbai, India). Cellulose microcrystalline (MCC) was obtained from Merck India, Mumbai. The compatibilizer polyethene-*graft*-maleic anhydride (PE-*g*-MA) and MMT K10 were received from Sigma-Aldrich, USA and used directly. Rice husk was collected from local rice mill industries of Assam. Other reagents used were of analytical grade.

2.2 Surface modification of RH

RH was treated with 2% soap solution at 70 °C for 1 h followed by washing with distilled water and finally drying in an oven at 100 °C for 12 h. The washed RH was dewaxed by treatment with a mixture of alcohol and benzene (1:2) for 72 h at 50 °C. It was washed with distilled water and dried for 12 h and then treated with 5% (w/v) NaOH solution for 30 min at 30 °C. It was then washed with distilled water for several times to leach out the absorbed alkali and finally kept immersed in distilled water overnight and were washed repeatedly to avoid the presence of any trace amount of alkali. The alkali-treated RH were dried in a vacuum oven at 70 °C for 12 h. The dried RH were grinded, passed though 50 mesh size sieve and stored at ambient temperature in a desiccator for further use.

2.3 Preparation of rice husk PVC nanocomposite (RHPNC)

35 phr of the modified RH was mixed with 60 phr of PVC, 5 phr of compatibilizer (PE-g-MA) different proportion of MCC/MMT (phr) and transferred to brabender plasticorder with mixing chamber of volume 100 cm^3 for blending. Initially, the above mixture was blended at a screw speed of 50–55 rpm at 70 °C for 3–4 min followed by the addition of LC and DBP. The final blending was carried out at 145 °C for 5 min at a screw speed of 70–75 rpm. The blended mixture was then compressed in compression moulding press (Santa) at 190 °C for 6 min under a pressure of 5–6 ton.

The formulation of the samples and their codification are given in Table 1.

3 Characterizations

The FTIR spectra were recorded for MCC, RH, MMT and composites with or without MMT in FTIR spectrophotometer (PerkinElmer, Frontier MIR-FIR, USA) using KBr pellet over the wavenumber range of 400–4000 cm^{-1}. The degree of distribution of MMC/MMT in the composite was evaluated by X-ray diffraction (XRD) analysis. It was carried out in a D8 FOCUS X-ray diffractometer (Bruker Axs, Germany) using Cu Kα radiation at a scanning rate of 1°/min with an angle ranging from $2\theta = 10°$ to 50°. The TEM investigations were carried on a JEM-2010 (JEOL) instrument equipped with a slow-scan CCD camera at an accelerating voltage of 200 kV. SEM analyses were carried out with

Table 1 Formulation of a mixture of samples (phr) and their codes

Sample code	PVC	RH	PE-g-MA	DBP	Lead carbonate	MCC	MMT
PRMCC0	60	35	5	5	5	0	5
PRMCC2	60	35	5	5	5	2	3
PRMCC4	60	35	5	5	5	4	1
PRMCC5	60	35	5	5	5	5	0

"JEOL, JSM Model 6390 LV" scanning electron microscope, operating at an accelerating voltage of 15 kV. The compatibility and morphological features of the composites were studied by using scanning electron microscope (JEOL JSM-6390LV) at an accelerated voltage of 5–10 kV. The fracture surface of the samples, deposited on a brass holder and sputtered with platinum, was used for this study. The DMA was performed under tension mode using a Mettler Toledo Instrument. The dimensions of the specimens were 10 mm × 10 mm × 5.5 mm. The specimens were scanned over a temperature range of 40–180 °C. Frequency of oscillation was fixed at 1 Hz and ramped at 2 k/min to 180 °C. Storage modulus, loss modulus, and mechanical loss factor (tan δ) were recorded and plotted against temperature. Thermal property of PVC, RH, MMT along with the polymer composite was measured in a thermogravimetric analyzer (TGA) (TGA-50, Shimadzu) at a heating rate of 10 °C/min up to 600 °C under nitrogen atmosphere at a flow rate of 30 mL/min. The tensile and flexural tests for composites were carried out at room temperature using universal testing machine (Zwick at a Z010, Germany) with a crosshead speed of 5 mm min^{-1} according to ASTM D-638 and D-790 respectively. Three samples of each category were tested, and their average values were reported. The hardness of the samples was measured according to ASTMD-2240 using a durometer (model RR12) and expressed as shore D hardness. Water vapour uptake (%) was measured by placing the samples in a humidity chamber at 65% relative humidity and maintaining a temperature of 30 °C. The weight and volume of the samples were measured at an interval of 6, 12, 24, 36, 48, 60, 72, 84 and 96 h. Water vapour uptake was determined using the following expression.

$$\text{Water uptake}\,(\%) = \left(W_s - W_1\right)/W_1 \times 100$$

where W_s is the weight of the specimen after water absorption and W_1 is the weight of the specimen before water absorption. LOI of the samples was measured by a flammability tester (S.C. Dey Co., Kolkata) according to the ASTM D-2863 method. The sample was placed vertically in the sample holder of the LOI apparatus. The ratio of nitrogen and oxygen at which the sample continues to burn for at least 30 s was recorded.

4 Results and discussion

4.1 FTIR

The FTIR spectra of MMT, PVC, MCC and composites with various percentage of MCC and MMT are shown in Fig. 1. In the spectrum of MMT (Fig. 1a), the strong absorption peak appeared at 3440 cm^{-1} was assigned to the –OH stretching frequency. Further, the small peak appeared around 3600 cm^{-1} might be due to the hydroxyl stretching vibration of aluminum or magnesium species present in MMT. The peak at 1638 cm^{-1} and 1048 cm^{-1} were due to the –OH bending and oxide band of metal. In the spectrum of PVC Fig. 1b, C–H and $–CH_2$ stretching modes were observed at 2860 cm^{-1} and 2977 cm^{-1}. The peak at 1428 cm^{-1} was assigned to the $–CH_2$ bending mode. Besides, peaks appeared at approximately at 1330, 1250, 950 and 830 cm^{-1} were due to CH_2 groups deformation, out of plane angular deformation, out of plane trans deformation and C–Cl bond stretching [38]. In the spectrum of MCC (Fig. 1c) the peak appeared at 3402 cm^{-1} was assigned for hydroxyl group and the absorption peak at 2904 cm^{-1} was due to symmetric C–H vibrations. The peaks at 1645 cm^{-1} (–OH bending), 1429 cm^{-1} ($–CH_2$ bending)

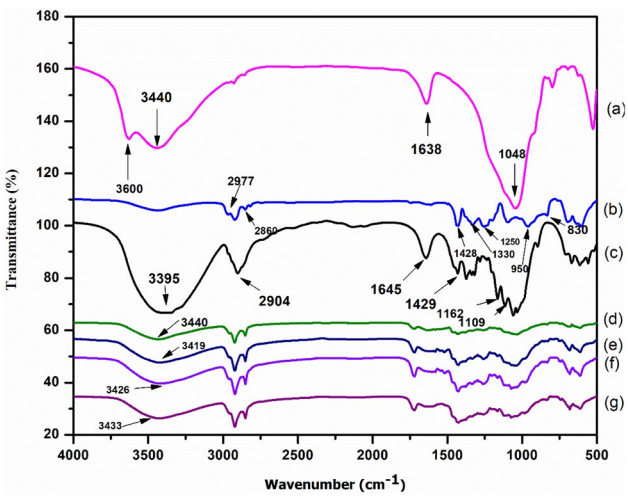

Fig. 1 FTIR spectra of (a) MMT (b) PVC (c) MCC (d) PRMMC0 (e) PRMMC2 (f) PRMMC4 (g) PRMMC5

and 1162 cm^{-1} (C–O stretching) were also appeared. The in-plane β-(1 → 4)-glycosidic linkage showed a peak at 1109 cm^{-1}. The band appeared in 685 cm^{-1} and 1100 cm^{-1} in the composites was due to O–Si–O stretching vibration [39]. In the spectrum of PRMCC0, the characteristic peaks of PVC and MMT were found. The spectra (Fig. 1e–g) shows the presence of peak at 1162 and 1109 cm^{-1} corresponding to C–O stretching and glycosidic linkage of cellulose. In the spectrum of composites (Fig. 1d–g) the intensity of the peaks corresponding to hydroxyl group was found more prominent compared to that of pure PVC. Compared to pure MCC the position of the hydroxyl peak was found to slightly shift towards lower wavenumber, suggesting a better interaction among different components including MCC and MMT. Further addition of MCC into the composite (Fig. 1f–g) showed a shifting of hydroxyl peak position towards higher wave number indicating a decrease in the interaction among various components. The intensity of peaks appeared at 2904 cm^{-1} due to symmetric OH vibration of MCC was found to increase as the percentage of MCC increased from 0 to 5 phr in the composites (Fig. 1d–g). All of these suggested an incorporation of both MCC and MMT in the composite.

4.2 XRD

The XRD curve of RH, PVC, MMT, MCC are shown in Fig. 2. The RH (curve 2a) had a little bit broad peak at 2θ = 22.3°, which was due to the cellulose present in RH. Similarly, the diffractogram of MCC (curve 2d) shows a sharp crystalline peak corresponding to 002 planes of crystalline cellulose at 2θ = 22.5°. Apart from this peak, MCC also shows characteristic peaks assigned to 101 and 040 planes of crystalline cellulose at 2θ = 14.6° and 34.3°

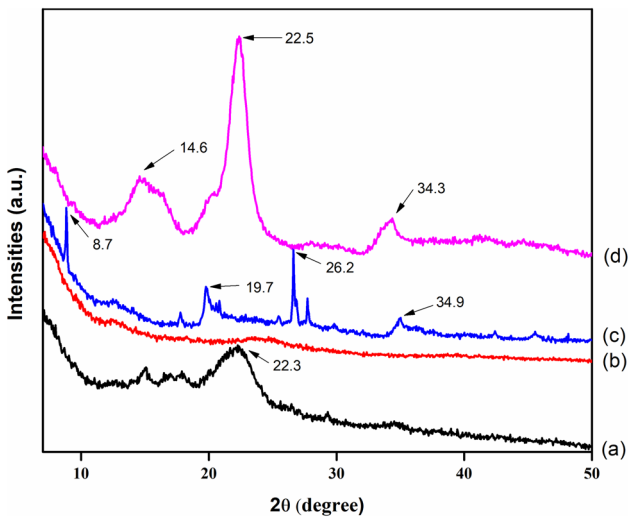

Fig. 2 XRD micrograph of (a) RH (b) PVC (c) MMT (d) MCC

[40]. These peaks confer the crystalline nature of MCC which corresponds to cellulose 1 polymorph structure [41]. MMT represented by curve 2(c) showed a characteristic peak at 2θ = 8.7°. The peak appeared at 2θ = 19.7°, 2θ = 26.2° and 2θ = 34.9° were due to the presence of silicate layers in the clay. PVC (Fig. 2b) did not show any remarkable peak because PVC is amorph material.

Figure 3a represents the XRD curves of the composite containing 0, 2, 4, 5 phr MCC. Fig. 3b represents the normalization curves of the samples (shown in Fig. 3a). In both the curves, the characteristic peak of MMT appeared at 2θ = 8.7° was not detectable in the composite. This could be either due to the full expansion of the clay gallery which was not possible to detect by XRD or delamination of the clay layers resulting in disappearance of crystal diffraction peak [42]. In the normalized figure, the peaks corresponding to MMT at 2θ = 19.7°, 26.2° and 34.9° were also decreased with the decrease in amount of MMT. This suggested the incorporation of PVC and other components into the interlayer spacing of MMT.

4.3 TEM

TEM study was performed to study the morphological characteristics of the prepared composite. The TEM micrograph shows the distribution of nano laminae of MMT in the nanocomposite as dark slice and MCC as dark spots. Figure 4a represents the composites without MCC. Here partial delamination of the MMT clay was observed. The micrograph containing 5 phr MCC (Fig. 4b) shows the presence of cellulose as dark spots. Few of the MCC particles were also agglomerated. The micrograph of PRMMC2 (Fig. 4c) containing 2 phr MCC and 3 phr MMT shows the presence of both MMT and MCC in the composite. The clay layers had been delaminated into thin lamellas by PVC and other components.

4.4 SEM

The SEM micrograph of the nanocomposite loaded with different percentage of MCC was shown in Fig. 5a–d. The rough surface (Fig. 5a) might be due to the agglomeration of MMT which resulted in the decrease in the interaction. The surface roughness decreased with an increased percentage of MCC in the composite. The decrease in surface roughness was maximum in the case of 2 phr MCC loaded composite (Fig. 5b). The roughness was found to increase again with further increase in MCC into the composite. This might be due to the agglomeration of MCC at higher dose.

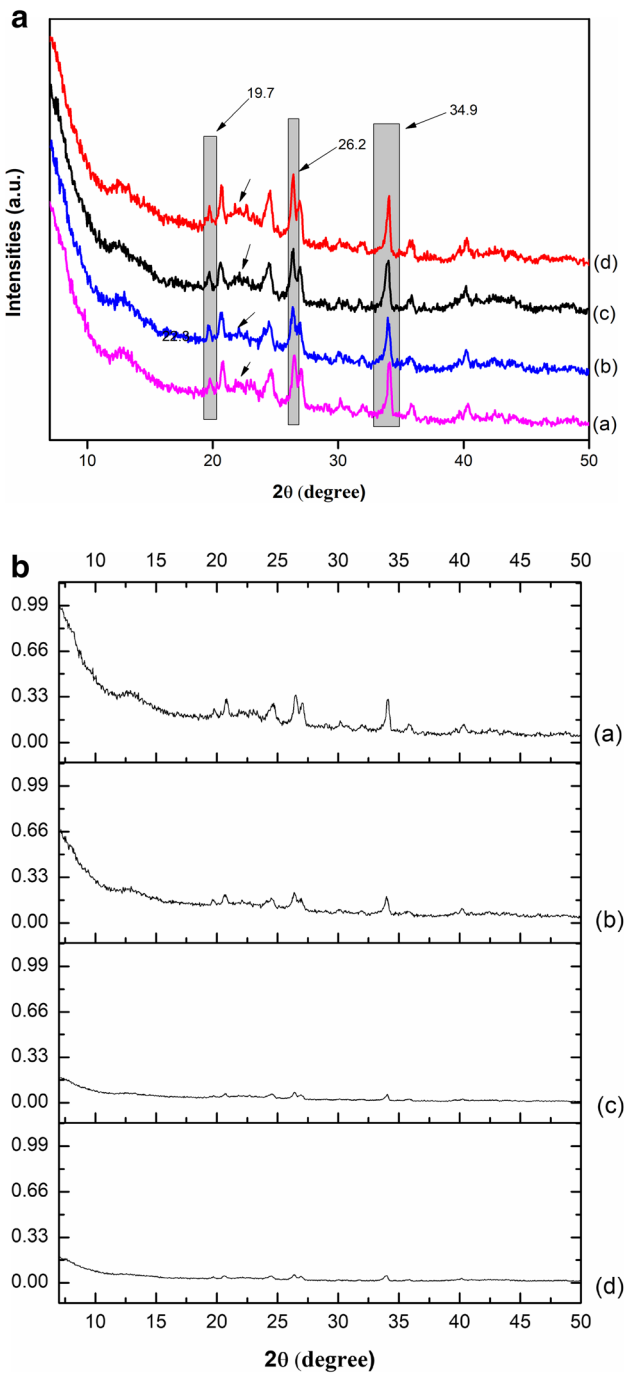

Fig. 3 **a** XRD micrograph of (a) PRMMC0 (b) PRMMC2 (c) PRMMC4 (d) PRMMC5. **b** Normalised XRD micrograph of (a) PRMMC0 (b) PRMMC2 (c) PRMMC4 (d) PRMMC5

4.5 DMA

4.5.1 Storage modulus

Figure 6 demonstrates the effect of incorporation of MCC and MMT on the storage modulus of PVC/RH composite. In all the composite, the storage modulus ($E^{/}$) found to decrease with the increase in temperature. It was evident from the Fig. 6 that the storage modulus was high below Tg, possibly due to the close and compact packing of the components. However, the $E^{/}$ curves show a sharp fall around 70–90 °C indicating glass/rubbery state transition. The increase in temperature enhanced the molecular mobility of the components of the composite which decreased the $E^{/}$ value in the rubbery region. However no significant changes were observed in $E^{/}$ value for all the composites in rubbery region. It was also observed that with the increase in the percentage of MCC into the composite, the value of storage modulus increased up to addition of 2 phr MCC and beyond that it decreased. This might be due to the increase in rigidity in the composites caused by the better dispersion of the reinforcing agents. Composites having 2 phr MCC and 3 phr MMT (Fig. 6b) showed high storage modulus. With the further increase in the amount of MCC, the value of storage modulus decreased probably due to poor dispersion of reinforcing agents which resulted in decrease of rigidity. With the increase in the percentage of MCC, a decrease in interaction was observed as revealed by FTIR study. The restricted movement of the polymer chains confined in the MMT layers also favored for showing higher storage modulus.

4.5.2 Loss modulus

Figure 7 illustrates the loss modulus of RH/PVC composites containing a various percentage of MCC and MMT as a function of temperature. Composites containing higher percentage of MCC (Fig. 7d) showed higher loss modulus. With the decrease in percentage of MCC and simultaneously with the increase in percentage of MMT in the composite the loss modulus was found to decrease (Fig. 7a–c). The change in loss modulus value could be explained based on synergistic effect of MCC and MMT. Both can influence the interfacial interaction between RH and PVC matrix. The loss modulus increased with the increase in temperature and after attaining a maximum, it decreased due to dissipation of energy caused by the relaxation of polymeric chains.

4.5.3 tan δ

Damping factor or tan δ of MCC/MMT containing RH/PVC composites are illustrated in Fig. 8. From the figure, it was evident that the damping factor increased with temperature, reaches peak in the transition region and then started decreasing. With increase in the percentage of MMT, a shifting of tan δ peak towards higher temperature was observed. The shifting of tan δ peak to higher temperature region or a decrease in intensity of the peak indicated an

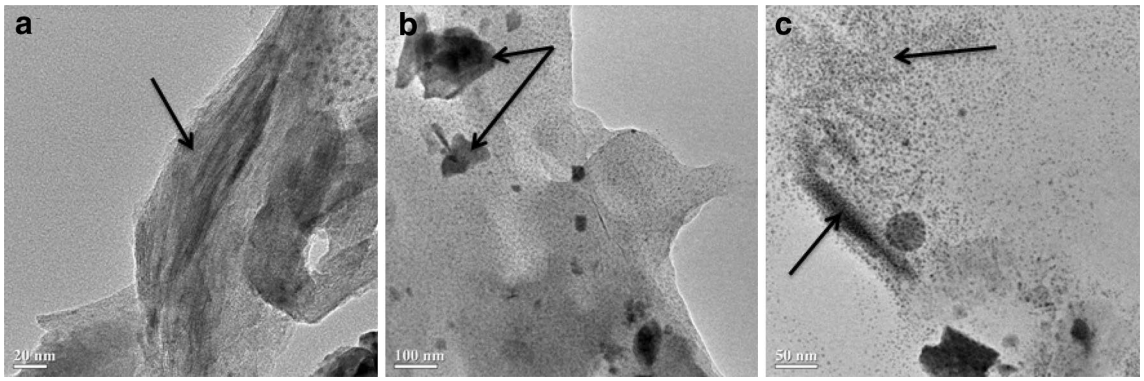

Fig. 4 TEM micrograph of **a** PRMMC0 **b** PRMMC5 **c** PRMMC2

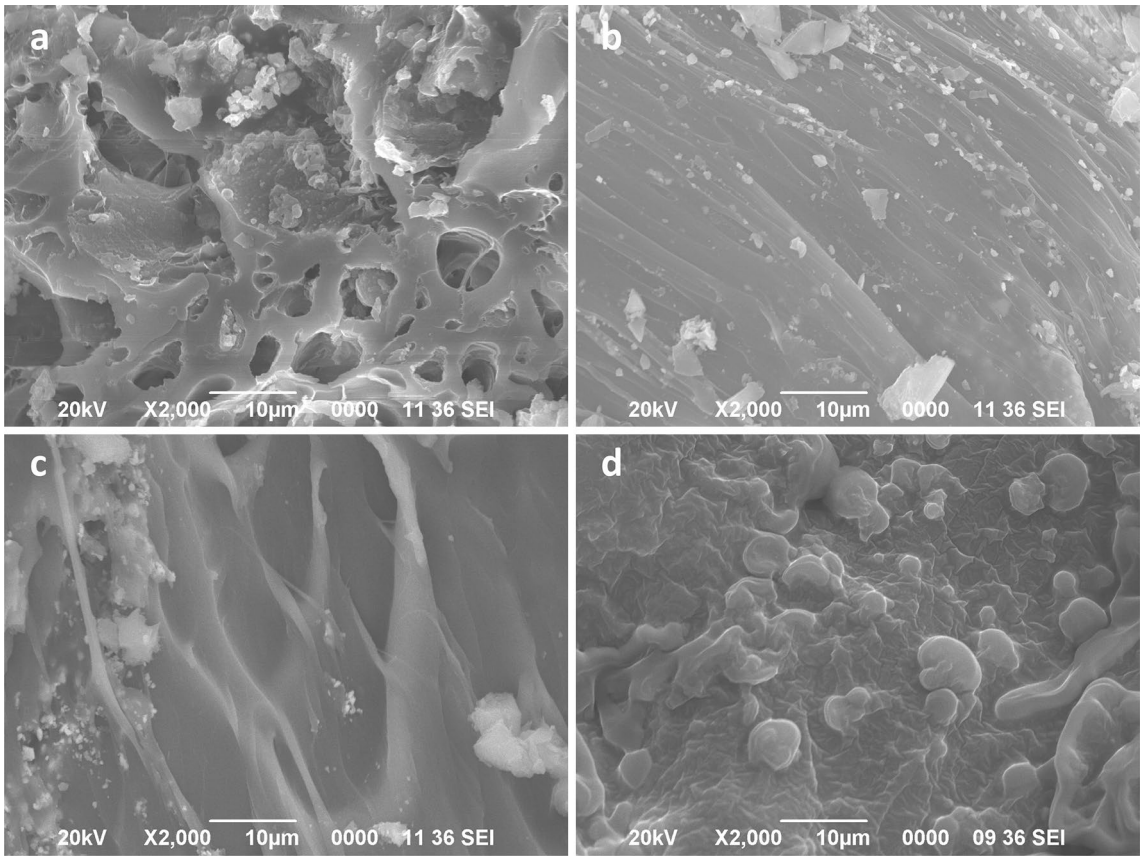

Fig. 5 SEM micrographs of **a** PRMMC0 **b** PRMMC2 **c** PRMMC4 **d** PRMMC5

increase in interaction among the components. In the case of sample PRMMC0 (curve a), although the shifting of tan δ peak was observed but there was no decrease in peak intensity. In all the other samples, a decrease in intensity was observed. The decrease in intensity probably played a major role in the case of PRMMC0 and hence its rigidity would be less compared to other samples. A shifting of tan δ peak indicating an increase in interaction among components was reported in the literature (Hristov and Vasileva 2003) [43]. Further, composites containing a combination of MCC and MMT (Fig. 8b, c) showed less intense peak compared to those of either MCC or MMT. This might be due to the restricted movement of the polymeric chains confined inside the clay layers [44]. Synergistic effect of MCC and MMT might be responsible for improving the interaction.

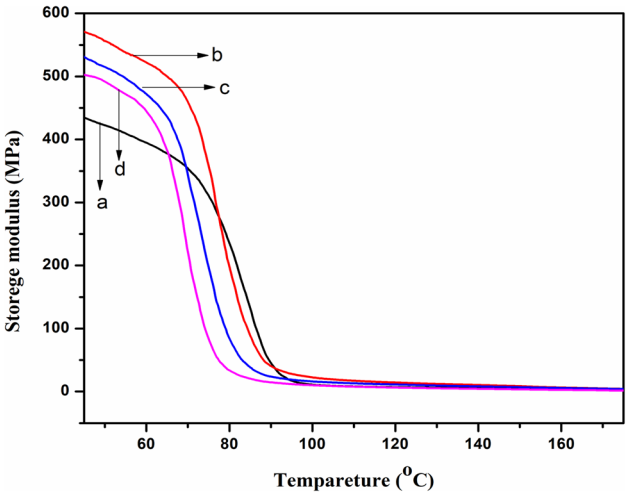

Fig. 6 Storage modulus of (a) PRMMC0 (b) PRMMC2 (c) PRMMC4 (d) PRMMC5

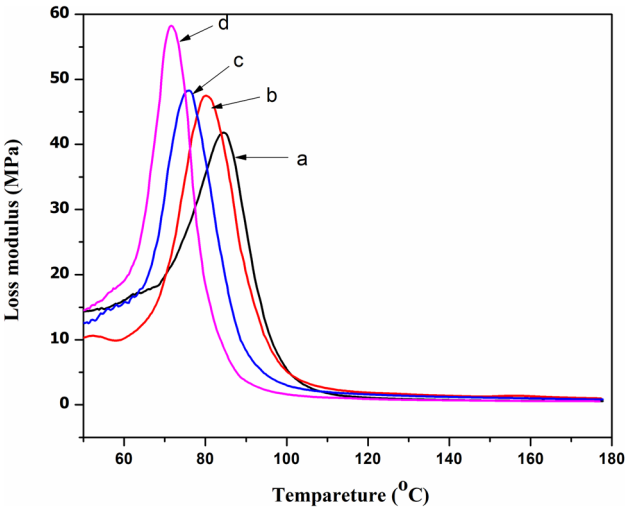

Fig. 7 Loss modulus of (a) PRMMC0 (b) PRMMC2 (c) PRMMC4 (d) PRMMC5

4.6 Thermal properties

Table 2 represents the thermograms of PVC, RH, MCC and composite with varying percentage of MCC and MMT. Table 2 shows the initial degradation temperature (Ti), maximum pyrolysis temperature (Tm), the temperature of decomposition at different weight loss (%) (T_D) along with residual weight (%) of PVC, RH, MCC and composites. MCC had a higher Ti value than PVC and RH which indicated a superior thermal resistance. The degradation of MCC was due to the decomposition of β-1,4-glucosidic linkage of cellulose chain [45]. Inclusion of MMT into the polymer matrix increases the Ti value. MCC showed one step degradation whereas RH, PVC and composites show

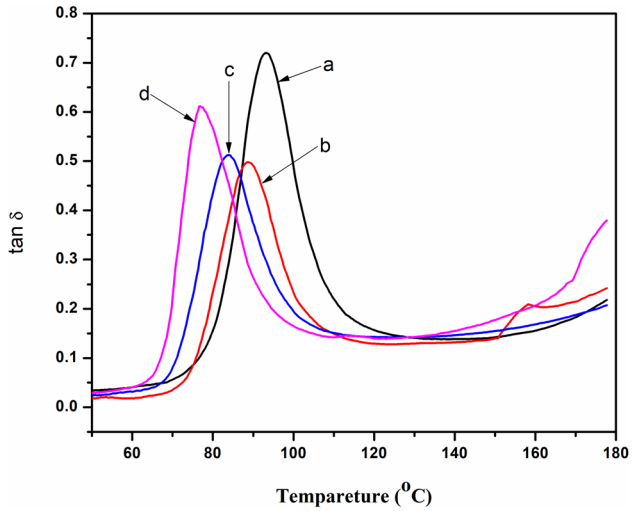

Fig. 8 tan δ of (a) PRMMC0 (b) PRMMC2 (c) PRMMC4 (d) PRMMC5

a two-step degradation. The T_m values for RH flour, PVC and composites might be attributed to the decomposition of α-cellulose for RH [46] and dehydrochlorination for PVC [47]. Introduction of MMT into the composite influenced the T_m value in the composite. T_m values for both the step increased up to the addition of combined nanofiller MCC/MMT in the ratio of 4:1, beyond that it decreased. A similar trend was also seen in the case of T_D values. The well-dispersed MCC and MMT in the polymer matrix enhanced the interaction among polymer matrix and RH, thereby delayed the decomposition of volatile matter. The decrease in thermal stability beyond the addition of 4 phr MCC might be due to the absence of MMT as well as agglomeration of MCC. The polymers were not able to be confined into the silicate layers due to the absence of MMT. Hence it might assist to easy passage of volatile components which resulted in decrease in thermal resistance. Sun et al. [48] reported that MCC got agglomerated at higher doses in the PVA/MCC matrix and hence affected various properties. The agglomeration decreased the interaction among PVC, RH and other components. The RW (%) values were also found high in the case of MCC/MMT (4:1) combined filler. The enhancement of RW value might be due to the presence of crystalline cellulose I from MCC and the char produced by MMT [49].

4.7 Mechanical and Hardness properties

The mechanical properties such as tensile strength, flexural strength of the PVC/RH/MMT/MCC hybrid nanocomposite with varying percentage of MCC and MMT are presented in Table 3. The results obtained in Table 3 were average values of 5 samples. All the mechanical properties were found to enhance with the increase in the presence

of MCC. The composite containing 2 phr MCC and 3 phr MMT showed higher mechanical properties suggesting a better interaction among the components in this combination. The improvement in the mechanical properties at this loading might be due to combined effect of MCC and MMT which reduced the mobility of the polymer chain [50]. Further increase in MCC loading decreased the values of mechanical properties which may be attributed to the agglomeration of the MCC in the composite. The agglomeration decreased the interfacial adhesion and increased the flexibility of the PVC chain leading to a decrease in both tensile and flexural properties. This suggested a better interaction of MCC with the polymer matrix than MMT. A similar trend was also observed for hardness property.

4.8 Limiting oxygen index test (LOI)

The LOI values of PRMMC composite with different MMT and MCC loadings are shown in Table 4. Composites having both MCC and MMT in the polymer matrix showed better LOI value than the composites having only either MCC or MMT component. Carbonaceous-silicate charred layer was formed during combustion on the surface of the composite, which acted as an insulation for the underlying material and retarded the heat transfer, i.e. delayed the decomposition rate [51]. The lower LOI value for both 5 phr MMT (PRMMC0) and MCC (PRMMC5) might be due to the poor dispersion and agglomeration of the component in the composite.

4.9 Water vapour uptake study

Figure 9 represents the water vapour uptake capacity of various composites with variation in MCC and MMT loading. The water vapour uptake capacity of the composites increased with time. Initially, the rate of moisture absorption was high, and then it slowed down. Water vapour uptake capacity of composites containing only MCC was higher than that of composites containing MMT alone. The trend of moisture absorption is PRMMC5 > PRMM0 > PRMMC4 > PRMMC2. The lowest water vapour uptake for composites containing MMT alone was due to the presence of silicate layers which hindered the penetration of water vapour into the composite [52]. On the other hand, composite having MCC showed highest water vapour uptake probably due to the formation of hydrogen bonding between MCC and water vapour.

Table 2 Thermal analysis of PVC, RH, MCC and PRMMC composite

Sample	Ti (°C)	Tm^a (°C)	Tm^b (°C)	Temperature of decomposition (T_D) in °C at different weight loss (%)				RW% at 600 °C
				20%	40%	60%	80%	
PVC	279	303	450	281	301	341	497	12
RH	265	293	–	265	306	423	–	31
MCC	343	345	–	322	341	349	357	7
PRMMC0	289	297	458	294	322	467	557	12
PRMMC2	291	308	461	301	326	464	–	30
PRMMC4	291	309	464	302	327	461	–	33
PRMMC5	282	297	456	288	311	413	534	10

Tm^a—T_m values for 1st step, Tm^b—T_m values for 2nd step

Table 3 Tensile, flexural and hardness properties of PRMMC

Sample name	Tensile strength (MPa)	Flexural strength (MPa)	Hardness (shore D)
PRMMC0	7.1 ± 0.09	37.31 ± 0.82	57 ± 4.3
PRMMC2	11.33 ± 0.09	38.16 ± 1.18	70 ± 5.5
PRMMC4	11.00 ± 0.39	35.17 ± 0.3	70 ± 6
PRMMC5	6.31 ± 0.07	31.25 ± 1.29	58 ± 4.3

Table 4 Limiting oxygen index (LOI) of RHPNC samples

Samples	LOI %	Flame description	Smokes and flames	Char
PRMMC0	46.7	Small localised flame	Small and black smoke	Medium
PRMMC2	50.0	Small localised flame	Small and black smoke	Medium
PRMMC4	50.0	Small localised flame	Small and black smoke	Medium
PRMMC5	44.4	Small localised flame	Small and black smoke	Medium

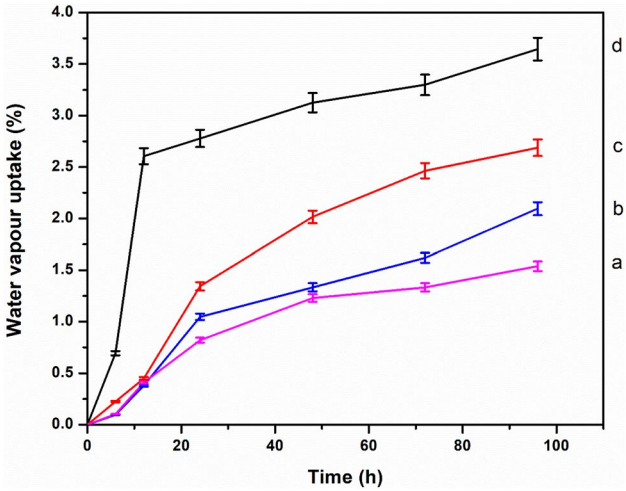

Fig. 9 Water vapor uptake of (a) PRMMC2 (b) PRMMC4 (c) PRMMC0 (d) PRMMC5

The moderate water uptake value by the composites might be due to the combined effect of filler (MMT/MCC) present in the composite.

5 Conclusion

In this study, polymer nanocomposites were prepared by a low-cost method where all the reinforcing components are derived from renewable bioresources like, RH, MCC and MMT. PVC was employed as the matrix. The ratio of MCC and MMT at which maximum interaction among various components occurred was 2:3 as shown by FTIR study. SEM study showed an increased in surface roughness with the increase in the ratio of MCC and MMT. Thermal stability of the composite was maximum at 4:1 ratio of MCC and MMT. Composites containing either MMC or MMT alone showed properties inferior to those of combined filler. Composites containing 2 phr MCC and 3 phr MMT showed an improvement in properties such as mechanical, flame retardancy and water vapour uptake due to synergistic effect. The surface morphology of the nanocomposite was also found to be improved in 2:3 MCC:MMT ratio.

Compliance with ethical standards

Conflict of interest On behalf of all authors, the corresponding author states that there is no conflict of interest.

References

1. Schneider JP, Myers GE, Clemons CM, English BW (1995) Biofibers as reinforcing fillers in thermoplastic composites. J Vinyl Addit Technol 1:103–108
2. Kato M, Usuki A, Okada A (1997) Synthesis of polypropylene oligomer-clay intercalation compounds. J Appl Polym Sci 66:1781–1785
3. Azwa ZN, Yousif BF, Manalo AC, Karunasena W (2013) A review on the degradability of polymeric composites based on natural fibres. Mater Des 47:424–442
4. Yousif BF, El-Tayeb NSM (2007) Tribological evaluations of polyester composites considering three orientations of CSM glass fibres using BOR machine. Appl Compos Mater 14:105–116
5. Joshi SV, Drzal LT, Mohanty AK, Arora S (2004) Are natural fiber composites environmentally superior to glass fiber reinforced composites? Compos A Appl Sci Manuf 35:371–376
6. Ahmad F, Choi HS, Park MK (2015) A review: Natural fiber composites selection in view of mechanical, light weight, and economic properties. Macromol Mater Eng 300:10–24
7. AL-Oqla FM, Sapuan SM (2014) Natural fiber reinforced polymer composites in industrial applications: feasibility of date palm fibers for sustainable automotive industry. J Clean Prod 66:347–354
8. Alves C, Ferrão PMC, Silva AJ et al (2010) Ecodesign of automotive components making use of natural jute fiber composites. J Clean Prod 18:313–327
9. Jamrichová Z, Aková E (2013) Mechanical testing of natural rubber composites for automotive industry, vol 7. https://ur.tnuni.sk/fileadmin/dokumenty/UR_V7_ISS3_20to25.pdf. Accessed 10 Sept 2018
10. Holbery J, Houston D (2006) Natural-fiber-reinforced polymer composites in automotive applications. JOM 58:80–86
11. Verheyen S, Blaton N, Kinget R, Kim H-S (2004) Thermogravimetric analysis of rice husk flour filled thermoplastic polymer composites. J Therm Anal Calorim 76:395–404
12. Han'guk Mokchae Konghakhoe H-J, Eom Y-G (2001) Journal of the Korean Wood Science and Technology, vol 29. The Korean Society of Wood Science Technology. https://www.koreascience.or.kr/article/ArticleFullRecord.jsp?cn=HMJGBP_2001_v29n3_59. Accessed 12 Sept 2018
13. Park BD, Gon Wi S, Ho Lee K, Singh AP, Yoon TH, Soo KY (2003) Characterization of anatomical features and silica distribution in rice husk using microscopic and micro-analytical techniques. Biomass Bioenerg 25:319–327
14. Soltani N, Simon U, Bahrami A, Wang X, Selve S, Epping JD, Pech-Canul MI, Bekheet MF, Gurlo A (2017) Macroporous polymer-derived SiO_2/SiOC monoliths freeze-cast from polysiloxane and amorphous silica derived from rice husk. J Eur Ceram Soc 37:4809–4820
15. Soltani N, Bahrami A, Pech-Canul MI, González LA (2015) Review on the physicochemical treatments of rice husk for production of advanced materials. Chem Eng J 264:899–935
16. Bahrami A, Pech-Canul MI, Soltani N, Gutiérrez CA, Kamm PH, Gurlo A (2017) Tailoring microstructure and properties of bilayer-graded Al/B4C/$MgAl_2O_4$ composites by single-stage pressureless infiltration. J Alloys Compd 694:408–418
17. Bahrami A, Soltani N, Pech-Canul MI, Gutiérrez CA (2016) Development of metal–matrix composites from industrial/agricultural waste materials and their derivatives. Crit Rev Environ Sci Technol 46:143–208
18. Šturcová A, Davies GR, Eichhorn SJ (2005) Elastic modulus and stress-transfer properties of tunicate cellulose whiskers. Biomacromol 6:1055–1061
19. Eichhorn SJ, Dufresne A, Aranguren M et al (2010) Review: current international research into cellulose nanofibres and nanocomposites. J Mater Sci 45:1–33
20. Azizi Samir MAS, Alloin F, Dufresne A (2005) Review of recent research into cellulosic whiskers, their properties and their application in nanocomposite field. Biomacromol 6:612–626

21. Petersson L, Oksman K (2006) Biopolymer based nanocomposites: comparing layered silicates and microcrystalline cellulose as nanoreinforcement. Compos Sci Technol 66:2187–2196
22. El-Sakhawy M, Hassan ML (2007) Physical and mechanical properties of microcrystalline cellulose prepared from agricultural residues. Carbohydr Polym 67:1–10
23. Uesu N (2000) Microcrystalline cellulose from soybean husk: effects of solvent treatments on its properties as acetylsalicylic acid carrier. Int J Pharm 206:85–96
24. Chuayjuljit S, Su-Uthai S, Charuchinda S (2010) Poly(vinyl chloride) film filled with microcrystalline cellulose prepared from cotton fabric waste: properties and biodegradability study. Waste Manag Res 28:109–117
25. Ma X, Chang PR, Yu J (2008) Properties of biodegradable thermoplastic pea starch/carboxymethyl cellulose and pea starch/microcrystalline cellulose composites. Carbohydr Polym 72:369–375
26. Auguello M, Ruszkay T, Reier GS (1998) Co-processed microcrystalline cellulose and calcium carbonate. EP 0942950. https://patents.google.com/patent/US4744987A/en. Accessed 15 Sept 2018
27. Arjmandi R, Teknologi U, Hassan A, Teknologi U (2014) Characterization of polylactic acid/microcrystalline cellulose/montmorillonite hybrid composites. Malays J Anal Sci 18:642–650
28. Sun J, Liang Y, Liu X, Liu Y (2018) Effects of replacement of part of the silica reinforcement with hybrid modified microcrystalline cellulose on the properties of their rubber composites. J Macromol Sci B Phys 57:243–254
29. Kozlowski R, Wladyka-Przybylak M (2008) Flammability and fire resistance of composites reinforced by natural fibers. Polym Adv Technol 19:446–453
30. Sathishkumar TP, Naveen J, Satheeshkumar S (2014) Hybrid fiber reinforced polymer composites—a review. J Reinf Plast Compos 33:454–471
31. Sathishkumar TP, Navaneethakrishnan P, Shankar S, Rajasekar R (2013) Characterization of new cellulose sansevieria ehrenbergii fibers for polymer composites. Compos Interfaces 20:575–593
32. Borba PM, Tedesco A, Lenz DM (2014) Effect of reinforcement nanoparticles addition on mechanical properties of SBS/curauá fiber composites. Mater Res 17:412–419
33. Yoonessi M, Toghiani H, Kingery WL, Pittman CU (2004) Preparation, characterization, and properties of exfoliated/delaminated organically modified clay/dicyclopentadiene resin nanocomposites. Macromolecules 37:2511–2518
34. Choy JH, Choi SJ, Oh JM, Park T (2007) Clay minerals and layered double hydroxides for novel biological applications. Appl Clay Sci 36:122–132
35. Chen G, Yao K, Zhao J (1999) Montmorillonite clay/poly (methyl methacrylate) hybrid resin and its barrier property to the plasticizer within poly(vinyl chloride) composite. J Appl Polym Sci 73:425–430
36. Zhao Y, Wang K, Zhu F, Xue P, Jia M (2006) Properties of poly(vinyl chloride)/wood flour/montmorillonite composites: effects of coupling agents and layered silicate. Polym Degrad Stab 91:2874–2883
37. Yang F, Hlavacek V (1999) Improvement of PVC wearability by addition of additives. Powder Technol 103:182–188
38. Ramesh S, Leen KH, Kumutha K, Arof AK (2007) FTIR studies of PVC/PMMA blend based polymer electrolytes. Spectrochim Acta A Mol Biomol Spectrosc 66:1237–1242
39. Soltani N, Bahrami A, Pech-Canul MI, González LA, Gurlo A (2018) Surface modification of rice-husk ash (RHA) by Si3N4 coating to promote its wetting by Al–Mg–Si alloys. Mater Chem Phys 203:223–234
40. Zhang J, Zhang B, Zhang J, Lin L, Liu S, Ouyang P (2010) Effect of phosphoric acid pretreatment on enzymatic hydrolysis of microcrystalline cellulose. Biotechnol Adv 28:613–619
41. Mathew AP, Oksman K, Sain M (2005) Mechanical properties of biodegradable composites from poly lactic acid (PLA) and microcrystalline cellulose (MCC). J Appl Polym Sci 97:2014–2025
42. Devi RR, Maji TK (2012) Study on properties of simul wood (*Bombax ceiba* L.) impregnated with styrene acrylonitrile copolymer, TiO_2, and nanoclay. Polym Bull 69:105–123
43. Hristov V, Vasileva S (2003) Dynamic mechanical and thermal properties of modified poly(propylene) wood fiber composites. Macromol Mater Eng 288(10):798–806
44. Devi RR, Mandal M, Maji TK (2012) Physical properties of simul (red-silk cotton) wood (*Bombax ceiba* L.) chemically modified with styrene acrylonitrile co-polymer and nanoclay. Holzforschung 66:365–371
45. Liu W, Fei M, Ban Y, et al. (2017) Preparation and Evaluation of Green Composites from Microcrystalline Cellulose and a Soybean-Oil Derivative. Polymers (Basel).9:541.
46. Johar N, Ahmad I, Dufresne A (2012) Extraction, preparation and characterization of cellulose fibres and nanocrystals from rice husk. Ind Crops Prod 37:93–99
47. Meng YZ, Tjong SC (1999) Preparation and properties of injection-moulded blends of poly(vinyl chloride) and liquid crystal copolyester. Polymer (Guildf) 40:2711–2718
48. Sun X, Lu C, Liu Y, Zhang W, Zhang X (2014) Melt-processed poly(vinyl alcohol) composites filled with microcrystalline cellulose from waste cotton fabrics. Carbohydr Polym 101:642–649
49. Haafiz MKM, Hassan A, Zakaria Z, Inuwa IM (2014) Isolation and characterization of cellulose nanowhiskers from oil palm biomass microcrystalline cellulose. Carbohydr Polym 103:119–125
50. Arjmandi R, Hassan A, Haafiz MKM, Zakaria Z (2015) Effect of microcrystalline cellulose on biodegradability, tensile and morphological properties of montmorillonite reinforced polylactic acid nanocomposites. Fibers Polym 16:2284–2293
51. Hazarika A, Mandal M, Maji TK (2014) Dynamic mechanical analysis, biodegradability and thermal stability of wood polymer nanocomposites. Compos B Eng 60:568–576
52. Yeh SK, Hsieh CC, Chang HC, Yen CCC, Chang YC (2015) Synergistic effect of coupling agents and fiber treatments on mechanical properties and moisture absorption of polypropylene–rice husk composites and their foam. Compos A Appl Sci Manuf 68:313–322